Monochromatization of synchrotron radiation for nuclear resonant scattering experiments

T.S. Toellner

Advanced Photon Source, Argonne National Laboratory, Argonne, IL 60439, USA

An introduction to monochromatization of synchrotron radiation in the energy range of 5–30 keV is presented for applications involving nuclear resonant scattering. The relevant relationships of the dynamical theory of X-ray diffraction are used to explain basic concepts of monochromatization. These relations are combined with ray-tracing techniques to design high-energy-resolution monochromators. Transmission-optimized and energy-resolution-optimized designs that achieve high energy resolutions ($10^6 < E/\Delta E < 10^8$) are discussed separately. Practical silicon monochromators of both types are presented for a variety of nuclear resonances in this energy range.

1. Introduction

Synchrotron radiation sources have evolved significantly over the last two decades and have given rise to new applications of X-ray scattering. Synchrotron sources are typically characterized by their spectral brilliance, which is expressed in units of photons/s/mrad^2/mm^2/0.1% bandwidth. Even within the narrow energy band of low-energy nuclear resonances, the spectral brilliance of present, third-generation synchrotron sources is many orders of magnitude greater than typical radioactive sources. This fact is due to the small size and exceptional collimation of these sources. The combination of high spectral brilliance with recently developed X-ray monochromatization techniques has fostered the development of nuclear resonant scattering, which takes advantage of low-energy nuclear resonances to obtain useful information about condensed matter systems.

Monochromatization involves extracting a given bandwidth of energies from the synchrotron radiation spectrum and has witnessed substantial progress in recent years. The recent developments have been twofold: efficient premonochromatization of raw synchrotron radiation in the presence of high thermal loads, and efficient, high-resolution monochromatization that takes advantage of the special properties of synchrotron radiation. Premonochromatization selects a particular spectral region of the available spectrum while mitigating the heat load. This keeps downstream optics, such as a high-resolution monochromator, from being overwhelmed. The development of efficient, high-resolution monochromators has relied on the availability of smaller, more collimated beams that are produced by undulators. These developments make experiments that demand higher energy resolution possible. Nuclear resonant scattering is

a prime example of an X-ray scattering technique that demands high-energy-resolution monochromatization and has benefitted enormously from these developments.

The desire to utilize synchrotron radiation sources to perform nuclear resonant scattering experiments has motivated attempts to improve monochromatization and has resulted in tremendous advances in terms of efficiency, tunability, and resolution. Nuclear resonant scattering involves the excitation of a very narrow energy nuclear resonance (10^{-7}–10^{-11} eV), while the synchrotron source produces an extremely broad spectrum of X-ray energies. As a result of this disparity in energy bandwidths and the fact that the raw X-ray beam can produce large thermal loads on the first monochromator, monochromatization is performed in two stages. The first monochromator, or premonochromator, is mainly designed to reduce the energy bandwidth to the level of $E/\Delta E \approx 10^4$ while mitigating the heat load. The second monochromator, or high-resolution monochromator, aims at reducing the energy bandwidth to as low as reasonably achievable while maintaining sufficient transmission to perform the intended experiment.

In the following, an introduction to monochromatization of synchrotron radiation in the energy range of 5–30 keV is presented for applications involving nuclear resonant scattering. In this energy range, monochromatization is achieved with Bragg diffraction from single crystals. Consequently, it will prove beneficial to begin with a summary of the basic relations relevant to Bragg diffraction from single crystalline materials. These basic relations together with geometric optics allow one to predict the effects of a combination of single crystals on synchrotron radiation. One may take advantage of this to produce a graphical representation of the behavior of multiple diffracting X-ray optics. This is carried out based on a restricted phase-space description that employs only the most relevant components of phase space: energy and angle. After these preliminary aspects, which are essential for a discussion of X-ray optics, we proceed to give a detailed description of two methods of achieving high-resolution monochromatization in this energy range.

2. Dynamical diffraction of X-rays

This section presents a brief summary of the relevant theoretical results of dynamical Bragg diffraction of X-rays from single crystals. The fundamental problem to be solved for X-ray diffraction involves finding the solutions to Maxwell's equations in a medium that possesses a spatially periodic complex dielectric function. By imposing the appropriate boundary conditions that are consistent with the Bragg condition, one can determine the scattered electromagnetic field both inside and outside the crystal. This was originally worked out by both Darwin [1] and Ewald [2] and later by von Laue [3]. Their results have been summarized by many authors [4–6].

For present purposes, it is sufficient if one considers Bragg diffraction in the two-beam case. Bragg diffraction implies that the radiation enters and exits through the same physical surface of the crystal. The two-beam case refers to the situation where only two points on the Ewald sphere are excited at the same time, corresponding to the

forward diffracted beam and a single Bragg-reflected beam. For Bragg diffraction in the two-beam case, the reflectivity for monochromatic radiation may be written as [7,8]

$$R(L) = L - \sqrt{L^2 - 1}, \tag{2.1}$$

where

$$\begin{aligned} L &= \frac{1}{1+\kappa^2}\left[W^2 + g^2 + \left[\left(W^2 - g^2 - 1 + \kappa^2\right)^2 + 4\left(gW - \kappa\right)^2\right]^{1/2}\right], \\ W &= \frac{1}{2}\left(\sqrt{b} + \frac{1}{\sqrt{b}}\right)\frac{\psi_{\mathrm{r}0}}{P|\psi_{\mathrm{r}H}|} + \sqrt{b}\,\frac{\sin 2\Theta}{P|\psi_{\mathrm{r}H}|}\,\theta, \\ g &= \frac{1}{2}\left(\sqrt{b} + \frac{1}{\sqrt{b}}\right)\frac{\psi_{\mathrm{i}0}}{P|\psi_{\mathrm{r}H}|}, \qquad \kappa = \frac{|\psi_{\mathrm{i}H}|}{|\psi_{\mathrm{r}H}|}. \end{aligned}$$

In this expression, the θ represents the angular deviation from the kinematical Bragg angle Θ. P is a factor describing the polarization of the incident radiation and equals 1 for σ-polarized (perpendicular to scattering plane) radiation and $\cos 2\Theta$ for π-polarized (parallel to scattering plane) radiation. $\psi_{(\mathrm{r,i})}$ are the real and imaginary parts of the complex susceptibility. The $\vec{H}$-components of the Fourier transform of $\psi_{(\mathrm{r,i})}$ are denoted by $\psi_{(\mathrm{r,i})H}$, where $\vec{H}$ represents a reciprocal lattice vector. Expressing these Fourier components of the susceptibility in terms of the structure of the crystal produces

$$\begin{aligned} \psi_{\mathrm{r}H} &= -\frac{r_\mathrm{e}\lambda^2}{\pi V}\sum_j \left(f_H + f'\right)\exp\left(2\pi\mathrm{i}\vec{H}\cdot\vec{R}_j\right)f_{\mathrm{DW}}^{(j)}\left(\vec{H}\right), \\ \psi_{\mathrm{i}H} &= -\frac{r_\mathrm{e}\lambda^2}{\pi V}\sum_j f''\exp\left(2\pi\mathrm{i}\vec{H}\cdot\vec{R}_j\right)f_{\mathrm{DW}}^{(j)}\left(\vec{H}\right), \end{aligned} \tag{2.2}$$

where V is the volume of the unit cell, r_e is the classical electron radius, and λ is the wavelength of the radiation. The sums are over the individual scattering factors of the atoms within the unit cell weighted by the relative phase due to the atom's location $\vec{R}_j$ within the unit cell. f_H is the $\vec{H}$-component of the Fourier transform of the electron density within a free atom and is typically calculated using self-consistent Hartree–Fock atomic wave functions. Values for f_H may be found in [9]. $f_{\mathrm{DW}}^{(j)}(\vec{H})$ represents the Debye–Waller factor for the jth atom and determines the reduction of the scattering strength due to lattice vibrations. For cubic crystals, such as silicon or germanium, relatively simple expressions for the Debye–Waller factor can be formulated (see, e.g., [9]). f' and f'' are the real and imaginary parts of a dispersion correction that results primarily from photoelectric absorption and becomes significant near atomic resonances. These may also be obtained from tables based on numerical calculations [10].

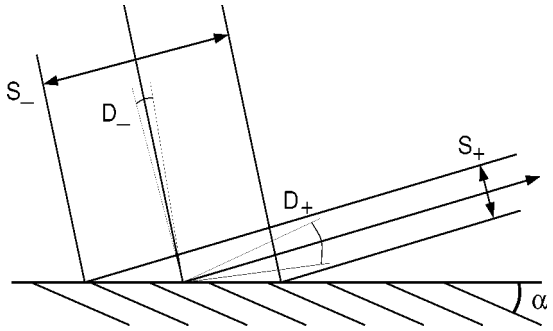

Figure 1. Incident ($-$) and diffracted ($+$) beam characteristics for X-rays diffracting from an asymmetric crystal reflection with the surface normal at an angle α with respect to the atomic layers. The convention adopted here defines the asymmetry angle such that the angle between the incident X-rays and the surface of the crystal is equal to $\Theta + \alpha$.

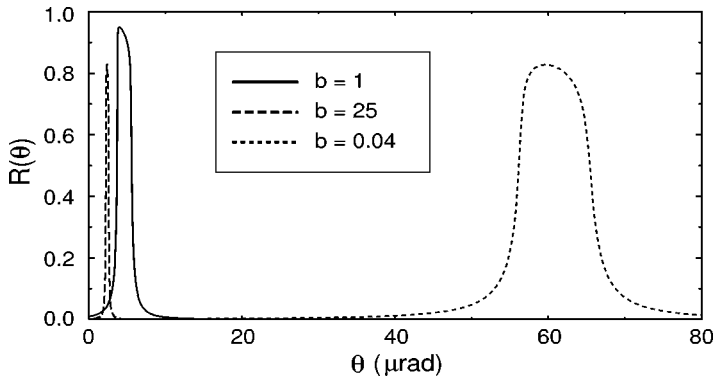

Figure 2. Reflectivity of a silicon (8 4 0) reflection for three different asymmetry factors (b) for 14.413 keV σ-polarized X-rays.

To account for the asymmetry that exists between the incident and diffracted wavefields when the atomic planes are not parallel to the physical surface, one has the asymmetry factor given by

$$b = \frac{\sin(\Theta + \alpha)}{\sin(\Theta - \alpha)}, \tag{2.3}$$

where the asymmetry angle α is the angle between the atomic planes and the physical surface of the crystal as defined in figure 1. Note that with this definition, b is always greater than 0 and $b = 1$ implies that the atomic planes are parallel to the physical surface. The reflectivity for a given reflection in crystalline silicon is plotted in figure 2 for three different values of the asymmetry factor. The angular spread of the reflectivity curve results from the extinction (i.e., removal from the forward beam) of X-rays as they scatter out of the crystal. As a result, X-rays scatter primarily from atoms within a certain depth, which is characterized by the extinction length, and only weakly from atoms located deeper in the lattice. Thus, the angular spread of the reflectivity curve

is related to the spatial spread of the atomic scatterers, weighted with their scattering contribution, through a Fourier transformation. In the case of a symmetric reflection, by which is meant that the atomic planes are parallel to the crystal surface, the angular width of the reflectivity curve is known as the Darwin width, given by

$$D = \frac{2}{\sin(2\Theta)} P|\psi_{\mathrm{r}H}|. \tag{2.4}$$

The angular width of the incident $(-)$ reflectivity curve for an asymmetric reflection is

$$D_- = \frac{D}{\sqrt{b}}, \tag{2.5}$$

while the angular width of the diffracted $(+)$ radiation is given by

$$D_+ = D\sqrt{b}. \tag{2.6}$$

A refraction effect due to the dispersion of the radiation as it propagates through the crystal lattice results in a shift of the nominal Bragg angle. For a symmetric reflection, this is given by

$$\Delta_{\mathrm{S}} = \frac{1}{\sin(2\Theta)} \psi_{\mathrm{r}0}, \tag{2.7}$$

where $\psi_{\mathrm{r}0}$ is obtained from eq. (2.2) with $\vec{H} = 0$. For an asymmetric reflection, the incident reflectivity curve experiences an angular shift of the nominal Bragg angle by an amount given by

$$\Delta_- = \frac{\Delta_{\mathrm{S}}}{2}\left(1 + \frac{1}{b}\right), \tag{2.8}$$

while the diffracted reflectivity curve experiences an angular shift of

$$\Delta_+ = \frac{\Delta_{\mathrm{S}}}{2}(1 + b). \tag{2.9}$$

The beam size plays a significant part in the design of high-resolution monochromators. In the case of a symmetric crystal reflection, the transverse size of the diffracted beam is determined by both the incident beam characteristics and the reflectivity profile of the diffracting crystal. In the case of an asymmetric reflection, the transverse size of the diffracted beam may be contracted or expanded by an additional factor that is simply the reciprocal of the asymmetry factor, b. Thus, the ratio of the transverse size (parallel to the scattering plane) of the diffracted beam (S_+) to that of the incident (S_-) accepted beam is given by

$$\frac{S_+}{S_-} = b^{-1}. \tag{2.10}$$

Equations (2.5), (2.6) and (2.10) demonstrate how a monochromatic X-ray beam may be manipulated. One can either produce a collimated beam with large size or a small

beam with increased divergence. This is illustrated in figure 1. As can be seen from Bragg's law, the beam divergence is intimately related to the energy resolution. The maximum allowable beam size that can be efficiently diffracted is limited by the ability to maintain good crystallinity over a long distance; hence the need for large single crystals. So, with the availability of large single crystals of silicon and the relatively small beam sizes that are offered by third-generation synchrotron sources, one is able to produce both a large angular acceptance with full spatial acceptance and high collimation. It will be shown that this fact can be used in designing monochromators to achieve high energy resolution while matching the angular acceptance of single crystals to the divergence of the radiation source.

3. Graphical approach to X-ray optics

How the optics in a synchrotron beam ultimately affect the characteristics of the transmitted radiation may be described with the use of phase space. Phase space, as a complete set of canonically conjugate variables, allows a full description of the time evolution of a dynamical system. Thus, one may use phase space as the framework for the description of the synchrotron radiation as it propagates through slits, mirrors, monochromators, and the like. For this purpose, a function $\vec{\mathcal{B}}(\vec{\tau})$ is introduced that represents the distribution of spectral brilliance, or the amount of energy in the radiation field (in units of quanta) per region of phase space at the phase-space location labelled by $\vec{\tau}$. Expressed in a linear polarization basis, the spectral-brilliance function is

$$\vec{\mathcal{B}}(\vec{\tau}) = \begin{pmatrix} \mathcal{B}_\sigma(\vec{\tau}) \\ \mathcal{B}_\pi(\vec{\tau}) \end{pmatrix}, \tag{3.1}$$

where $\sigma(\pi)$ represents the transverse polarization component that is parallel (perpendicular) to the orbit plane of the synchrotron. The phase-space coordinate $\vec{\tau}$ may be described as a vector with components given by

$$\vec{\tau} = \begin{pmatrix} x_{\mathrm{v}} \\ x_{\mathrm{h}} \\ \theta_{\mathrm{v}} \\ \theta_{\mathrm{h}} \\ \varepsilon \end{pmatrix}, \tag{3.2}$$

where $x_{\mathrm{v(h)}}$ is the vertical (horizontal) position, $\theta_{\mathrm{v(h)}}$ is the vertical (horizontal) angular deviation (normalized transverse momentum), and ε is the relative energy (i.e., $\varepsilon = E - E_0$). In general, an optic has appreciable transmission only in some restricted phase-space volume, and radiation incident outside that volume does not get transmitted through the optic or is significantly suppressed. The size of that volume along different directions in phase space is referred to as acceptance, e.g., vertical (horizontal) spatial acceptance and vertical (horizontal) angular acceptance. For monochromators diffracting in the vertical plane as will be described here, one simply refers to spatial

and angular acceptance to refer to the vertical components. The horizontal components are of negligible importance for small, well-collimated beams.

The relevant effects of introducing an element, such as a single crystal lattice reflection, may be characterized by a transmission function $\mathbf{T}(\vec{\tau})$ together with a coordinate map $\mathbf{A}$. The coordinate map describes the redistribution of radiation in phase space. For example, it depicts effects such as focusing, collimation, and so on. The transmission function determines the reduction in spectral brilliance at a phase-space point due to absorption and other processes that scatter radiation out of the initial phase-space volume and are considered as losses. The spectral-brilliance function after an X-ray element then has the following form:

$$\vec{\mathcal{B}}'\left(\vec{\tau}'\right) = \vec{\mathcal{B}}'(\mathbf{A}\vec{\tau}) = \mathbf{T}(\vec{\tau})\vec{\mathcal{B}}(\vec{\tau}), \tag{3.3}$$

where the transmission function as expressed in a linear polarization basis has a matrix representation

$$\mathbf{T} = \begin{pmatrix} T_{\sigma\sigma} & T_{\sigma\pi} \\ T_{\pi\sigma} & T_{\pi\pi} \end{pmatrix}. \tag{3.4}$$

In order to consider a series of diffracting elements, one may generalize eq. (3.3) to n diffracting elements by recursion to obtain

$$\begin{aligned}
\vec{\mathcal{B}}_1(\mathbf{A}_1\vec{\tau}) &= \mathbf{T}_1(\vec{\tau})\,\vec{\mathcal{B}}_0(\vec{\tau}), \\
\vec{\mathcal{B}}_2(\mathbf{A}_2\mathbf{A}_1\vec{\tau}) &= \mathbf{T}_2(\mathbf{A}_1\vec{\tau})\,\mathbf{T}_1(\vec{\tau})\,\vec{\mathcal{B}}_0(\vec{\tau}), \\
\vec{\mathcal{B}}_3(\mathbf{A}_3\mathbf{A}_2\mathbf{A}_1\vec{\tau}) &= \mathbf{T}_3(\mathbf{A}_2\mathbf{A}_1\vec{\tau})\,\mathbf{T}_2(\mathbf{A}_1\vec{\tau})\,\mathbf{T}_1(\vec{\tau})\,\vec{\mathcal{B}}_0(\vec{\tau}), \\
&\vdots \\
\vec{\mathcal{B}}_n\left(\prod_{i=1}^{n}\mathbf{A}_i\vec{\tau}\right) &= \underbrace{\left[\prod_{i=1}^{n}\mathbf{T}_i\left(\prod_{j=1}^{i-1}\mathbf{A}_j\vec{\tau}\right)\right]}_{\substack{\text{Transmission}\\ \text{function}}}\vec{\mathcal{B}}_0(\vec{\tau}),
\end{aligned} \tag{3.5}$$

where $\mathbf{T}_i$ and $\mathbf{A}_i$ are the transmission function and the coordinate map for the ith element and $\vec{\mathcal{B}}_i$ is the spectral-brilliance function after the ith element. The bracketed expression represents the overall transmission function of the entire set of elements.

An approximate transmission matrix for a Bragg diffracting single crystal can be constructed for the sake of calculating the transmission characteristics of a multi-element X-ray monochromator. Assuming polarization switching to be negligible for energies far away from atomic resonances, this is simply

$$\mathbf{T} = \begin{pmatrix} T_{\sigma\sigma} & T_{\sigma\pi} \\ T_{\pi\sigma} & T_{\pi\pi} \end{pmatrix} \approx \begin{pmatrix} R_{\sigma} & 0 \\ 0 & R_{\pi} \end{pmatrix}. \tag{3.6}$$

The components of the transmission matrix depend on the scattering mechanism of the radiation in the given medium. In the case of radiation Bragg scattering from a crystalline material, the transmission matrix elements may be calculated from the theory of dynamical diffraction of X-rays (cf. eq. (2.1)).

To represent the acceptance of an X-ray element to synchrotron radiation graphically, one may plot the transmission function in the incident coordinates. Since the phase-space region as described here has five dimensions, some components must be disregarded in order to display the function graphically. The most useful components for present purposes are θ_v and ε. Consequently, it is beneficial to adopt a restricted phase-space approach by considering only two components of phase space – energy and angle. Within this restricted phase space, the coordinate map becomes [11]

$$\mathbf{A} \approx \begin{pmatrix} \pm b & \dfrac{\pm(1-b)}{E_0 \cot\Theta} \\ 0 & 1 \end{pmatrix}, \qquad \vec{\tau} = \begin{pmatrix} \theta_\mathrm{v} \\ \varepsilon \end{pmatrix}. \tag{3.7}$$

The $\pm$ refers to whether the crystal reflection is in a $(+,+)$ or $(+,-)$ scattering geometry relative to the previous crystal reflection. The $(+,+)$ scattering geometry implies that the scattering angle of the beam due to the second crystal reflection is in the same rotation direction as that due to the first crystal reflection. On the other hand, a $(+,-)$ scattering geometry would imply that the scattering angle of the beam due to the second crystal reflection is in the opposite rotation direction as that due to the first crystal reflection.

Equations (3.5)–(3.7) taken together allow a three-dimensional graphical representation of the transmission function, from which one may visualize the energy acceptance, angular acceptance, and transmission of the diffracting system. Furthermore, it is possible to calculate other quantities that are useful for determining the characteristics of an optic. These include the energy-dependent, angle-integrated transmission, which gives an estimate of the energy resolution, and the (totally) integrated transmission, which gives an estimate of the efficiency, or throughput.

For calculating observable quantities, such as the energy-resolution function of a monochromator or the flux of radiation after an optic, it is necessary to include the spectral-brilliance function of the source ($\vec{\mathcal{B}}_0(\tau)$ in eq. (3.5)). This characterizes the properties of the source and is often responsible for the same optic giving slightly different results when used with different sources. The present use of a restricted phase space means that the spatial components of the spectral-brilliance function are integrated, resulting in a new quantity known as the spectral-brightness function,

$$\vec{B}(\theta_\mathrm{v}, \theta_\mathrm{h}, \varepsilon) = \int \vec{\mathcal{B}}(x_\mathrm{v}, x_\mathrm{h}, \theta_\mathrm{v}, \theta_\mathrm{h}, \varepsilon)\, \mathrm{d}x_\mathrm{v}\, \mathrm{d}x_\mathrm{h}. \tag{3.8}$$

In general, the spectral-brightness function represents the distribution of spectral brightness as a function of energy and both vertical and horizontal angles. For our purposes, the horizontal angle will be suppressed in the sense that the radiation will be considered to be horizontally collimated. This is a reasonable assumption for third-generation synchrotron sources, and has a negligible effect on the simulation of measured results due to the fact that diffraction is assumed to be in the vertical plane and is thus only weakly dependent on horizontal angular deviations. The notation will reflect this stipulation only through the listing of the dependent variables such that

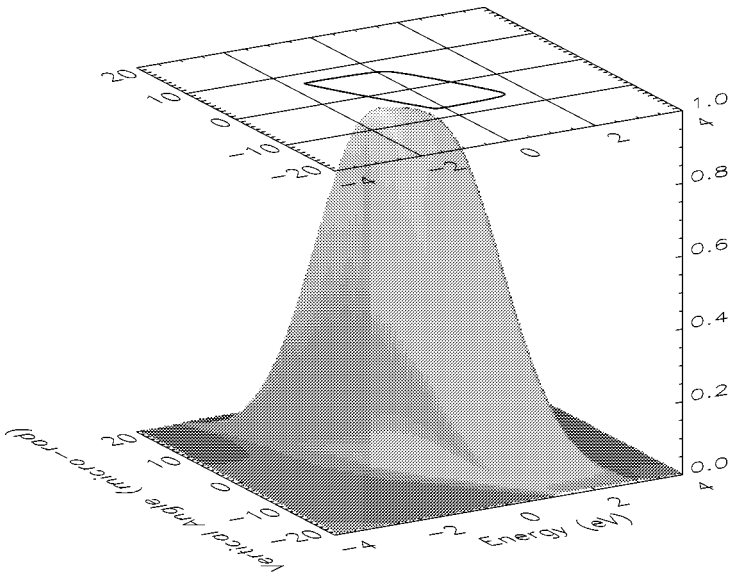

Figure 3. Spectral-brightness function (normalized) $B_\sigma(\theta, \varepsilon)$ around $E_0 = 14.413$ keV that includes the transmission function for two silicon (1 1 1) crystal reflections in a $(+,-)$ scattering geometry. In the ideal case, this is the distribution of σ-polarized radiation after such a monochromator.

$\vec{B}(\theta_\mathrm{v}, \varepsilon) \equiv \vec{B}(\theta_\mathrm{v}, \theta_\mathrm{h}, \varepsilon)|_{\theta_\mathrm{h}=0}$. Also, the subscript "v" will be omitted from the angle variable assuming that all angular references refer to the vertical angle. Figure 3 shows a plot of a spectral-brightness function (normalized to the incident on-axis spectral brightness) from a typical third-generation undulator source that includes the transmission function of two silicon (1 1 1) lattice reflections in a $(+,-)$ scattering geometry at 14.413 keV. In the ideal case, this is the distribution of σ-polarized radiation after such a monochromator.

4. High-resolution monochromatization

In the following, various methods of filtering narrow spectral bands from premonochromatized synchrotron radiation are examined. The primary task of a high-resolution monochromator is to minimize the energy bandwidth of the transmitted radiation while maintaining an acceptable transmission of the available spectral flux. Thus, the monochromator must have a spatial and angular acceptance that is matched to the size and divergence of the incident radiation. For nuclear resonant scattering experiments using synchrotron radiation, the monochromator must accommodate the radiation from insertion devices where the radiation source may be characterized as having a high spectral brilliance. For the present third-generation synchrotron sources, this means that the incident radiation is concentrated within a small (vertical size ≈ 1 mm) and highly collimated (vertical divergence ≈ 15 μrad) beam. Because high resolution monochromatization follows the premonochromatization stage, the issue of

an enormous concomitant heat load is mostly eliminated. At present synchrotron sources, however, a premonochromatized ($E/\Delta E \approx 10^4$) X-ray beam is sufficiently intense to still produce heat loads that are in the range of 10^{-2}–10^{-1} W – a mini-heat-load. At the level of energy resolutions that are presented here, and at the X-ray intensities presently available, this mini-heat-load is noticeable. As the intensity of sources increases and as resolutions are pushed higher, this load may become serious.

There are a number of specific methods for achieving high resolution that have their respective advantages and disadvantages depending on the actual application. One method involves using a single diffraction from a lattice of a pure crystalline material with a Bragg angle that is close (within mradians) to $\pi/2$ radians. This backscattering geometry produces energy resolutions that cover the range of $E/\Delta E \sim 10^5$–10^8 in the X-ray region of 5–30 keV. Furthermore, back reflections possess significantly increased angular acceptances in this energy range [12]. So, one might well ask whether back reflections may be used for monochromatization at nuclear resonance energies. Since reciprocal lattice vectors ($\vec{H}$) take on only discrete values in a crystal, back reflections are only possible at discrete energies. Applications involving nuclear resonant scattering restrict the monochromatization to certain discrete energies as well, and typically, nuclear resonance energies in this energy range do not coincide with back-reflection energies for high-quality crystalline materials like silicon, or germanium, at room temperature. It is possible to adjust the temperature of the crystalline material to change the lattice constant and consequently, to change the back-reflection energy. This only produces small shifts in the back-reflection energy, so the room temperature back-reflection energy must already be close to the nuclear resonance energy in order for this to be a viable option. Alternatively, one can choose a crystalline material with a room-temperature lattice constant that provides a better match between the back-reflection energy and the nuclear resonance energy. Also, cubic crystalline materials like silicon and germanium, which have the diamond structure, belong to a crystal class of high symmetry. Consequently, many of the lattice reflections are either forbidden or degenerate (possessing the same d-spacing and hence, the same back-reflection energy). By choosing a crystalline material with lower crystal symmetry like Al_2O_3, which is hexagonal, one has many more lattice reflections available. Such investigations into the behavior and possibility of using Al_2O_3 as a backscattering monochromator have only recently been undertaken [13]. Backscattering is a method that is indispensable for sources that have a large divergence, e.g., as energy analyzers in an inelastic X-ray scattering experiment [14]. For small X-ray beams with low divergence, multicrystal arrangements provide greater flexibility from the standpoint of beam separation and the ability to select the diffraction energy. Furthermore, in this energy range, multicrystal monochromators provide an opportunity to achieve higher energy resolutions.

In the following section, different high-resolution monochromators composed of two separate crystalline silicon blocks are presented. Depending on the mean energy of the incident radiation, two different approaches to high-resolution monochromators in this energy range provide both good angular acceptance as well as good energy

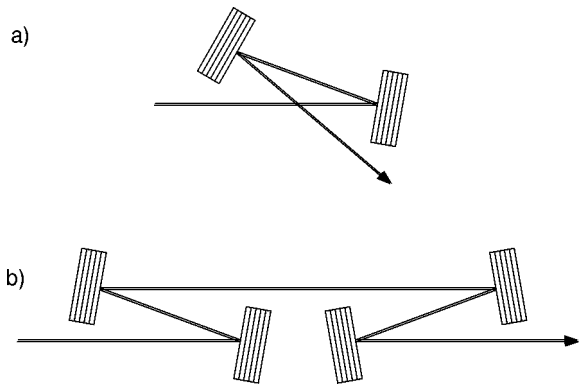

Figure 4. Monochromator design giving high energy resolution but with low transmission: (a) two symmetrically cut high-order reflections placed in a (+h, +h) scattering geometry, and (b) a four-reflection version based on the same principle, but which redirects the beam to the forward direction.

resolution. These two approaches involve utilizing different crystal reflections and are both presented along with criteria for their performance and fabrication.

4.1. Transmission-optimized design

The use of two high-order, symmetrically cut crystal reflections in a $(+\mathrm{h}, +\mathrm{h})$ scattering geometry offers good energy resolution [15]. This arrangement along with a four-reflection version that has the advantage of preserving the beam direction is shown in figures 4(a) and 4(b). In the energy range of 10–30 keV, silicon crystal reflections with large Bragg angles possess Darwin widths that are exceedingly small – on the order of a few μradian at 10 keV and decreasing to sub-μradian above 20 keV. This presents a problem for the use of high-order crystal reflections for high-resolution monochromatization, because the mismatch between crystal Darwin widths and the source divergence of present-day sources results in low transmission. To overcome this obstacle, one can collimate the incident radiation by first diffracting from a crystal reflection that is asymmetrically cut. From eqs. (2.5) and (2.6), the ratio between the angular spread of the diffracted radiation to that of the angular acceptance is equal to the asymmetry factor, b. Thus, a crystal reflection with an asymmetry factor b will collimate the incident radiation by that same factor. Therefore, one may improve the overall transmission of a crystal reflection that has a large Bragg angle if one first diffracts the synchrotron radiation from a crystal reflection with an asymmetry factor that is less than one. From eq. (2.10), a crystal reflection with an asymmetry factor b will also alter the size of the diffracted beam (parallel to the diffraction plane) by the factor b^{-1} relative to its spatial acceptance. In addition, the crystals must be placed in a $(+, +)$ scattering geometry as shown in figure 5(a) to achieve the energy-bandwidth reduction. The essence of this design was proposed as a means of achieving high energy resolution with large angular acceptance [16] for improving the signal-to-noise ratio in nuclear resonant scattering experiments with synchrotron radiation.

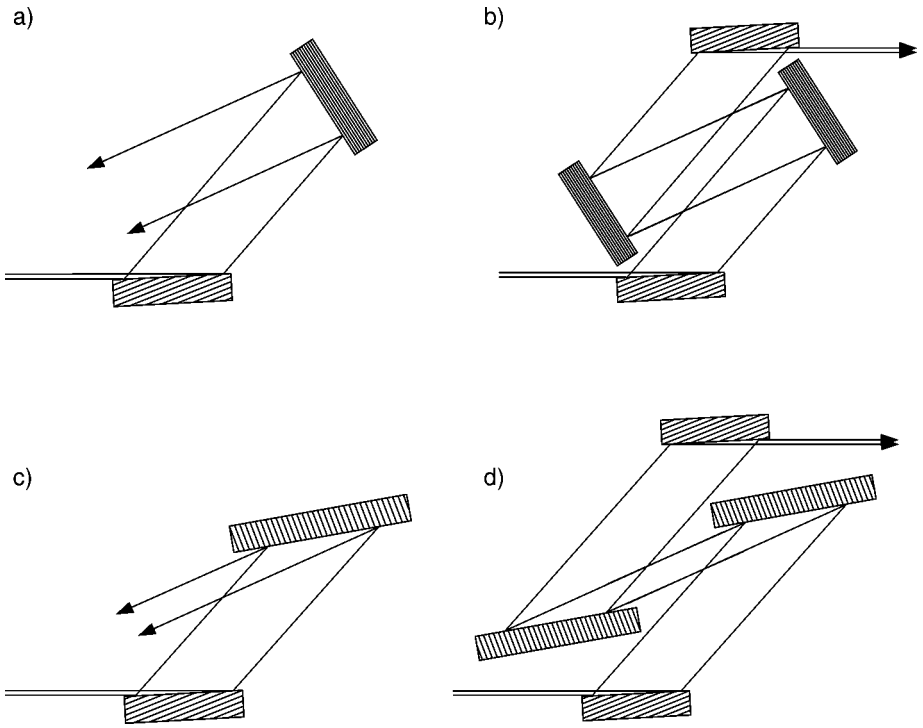

Figure 5. High-resolution monochromators optimized for transmission: (a) first crystal reflection (low order) is asymmetrically cut, while the second (high order) crystal reflection is symmetrically cut, (b) a four-reflection version of (a) that redirects the beam to the forward direction, (c) first reflection (low order) is asymmetrically cut and second reflection (high order) is also asymmetrically cut, but in the opposite sense, and (d) a four-reflection version of (c) that redirects the beam to the forward direction.

Choosing which crystal reflections to use so as to optimize this two-crystal arrangement depends on many factors. First, assuming there is no back reflection available, the crystal reflection possessing the largest Bragg angle at the desired energy should be chosen as the second diffracting crystal. Second, the first crystal reflection should be chosen such that its Darwin width (D_1) is equal to the geometric mean of the incident monochromatic divergence – the smaller of either source divergence or an upstream crystal Darwin width – and the Darwin width of the second diffracting crystal,

$$D_1 \equiv \sqrt{\eta D_2}, \tag{4.1}$$

where D_2 is the Darwin width of the second diffracting crystal and η is the incident monochromatic divergence. By choosing the first crystal reflection in this way, an appropriate asymmetry factor may then be determined from the relation

$$b_1 \equiv \frac{D_2}{\eta}. \tag{4.2}$$

The actual angles between the atomic planes and the physical surface of the crystal are then determined from eq. (2.3). Thus, in accordance with eqs. (2.5) and (2.6), the first crystal collimates the incident beam down to the Darwin width of the second diffracting crystal.

The procedure outlined above for choosing the crystal reflections and their asymmetry factors works fairly well if eq. (4.2) does not result in extreme values for the asymmetry factor. Small values for the asymmetry factor result in diffracted beam sizes that become exceedingly large, thus requiring crystallinity over large distances for both crystal blocks. It should be noted that the long-range crystallinity depends on such factors as strain and temperature, and thus the use of large crystal blocks should be avoided when possible. In addition, extreme values for the asymmetry factor also result in decreased reflectivity. In the situation where the asymmetry factor is too small to ensure the performance of the two-crystal arrangement, one may instead fix the asymmetry factor at some reasonable value and then determine the appropriate crystal reflection based on the following relationship:

$$D_1 \equiv \frac{D_2}{\sqrt{b_1}}. \tag{4.3}$$

One may further reduce the transmitted energy bandwidth by reducing the angular acceptance of the second crystal reflection via an asymmetrically cut surface [17]. This may require greater collimation of the incident radiation by the first crystal reflection, i.e., the asymmetry factor of the first crystal reflection may have to be reduced further. To explore the effect that an asymmetry factor on the second crystal has on resolution and transmission of a two-crystal arrangement, one can simulate the angle-integrated transmission as a function of energy. Figure 6 demonstrates just this case assuming

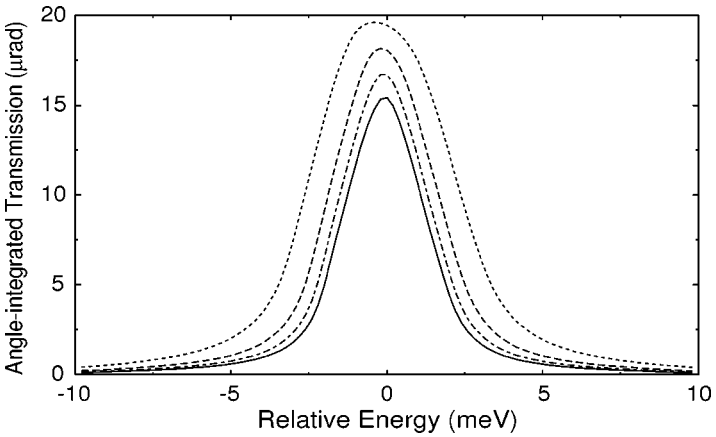

Figure 6. Angle-integrated transmission $\int T_\sigma(\theta,\varepsilon)\,\mathrm{d}\theta$ as a function of energy (relative to 14.413 keV) for an asymmetrically cut silicon (4 4 0) reflection ($b_1 = 0.04$) followed by an asymmetrically cut silicon (9 7 5) reflection in a $(+,+)$ scattering geometry as shown in figure 5(c). The asymmetry factor for the second crystal reflection has the values $b_2 = 1, 2, 3, 4$, with $b_2 = 4$ yielding the narrowest transmitted energy bandwidth.

Table 1
Silicon two-crystal high-resolution monochromators of a transmission-optimized design for different nuclear resonances in the energy range of 10–30 keV. The chosen reflections ($\vec{H}$) and asymmetry angles (α) should be considered representative rather than optimal.

Isotope	E_0 (keV)	$\vec{H}$ (h k l)	Θ_B (deg.)	α^a (deg.)	s^b (mm)	ΔE (meV)	$\Delta\Theta$ (μrad)	$\int T_\sigma \, \mathrm{d}\theta^c$ (μrad)	$\int T_\sigma \, \mathrm{d}\theta \, \mathrm{d}\varepsilon^c$ (nrad-eV)	δT_0 (mK)
^{57}Fe	14.413	(4 4 0)	26.62	−24.7	21	3.4	22	16.0	64.8	92
		(9 7 5)	80.40	+71.0	35					
^{151}Eu	21.542	(4 4 0)	17.44	−16.0	40	1.0	13	9.3	11.5	18
		(15 11 3)	86.72	0.0	71					
^{149}Sm	22.494	(4 4 4)	20.58	−19.0	36	0.7	8.3	5.0	4.2	12
		(13 13 7)	86.62	+74.0	70					
^{119}Sn	23.880	(4 4 4)	19.34	−18.0	43	1.1	8.2	5.3	6.8	18
		(12 12 12)	83.46	0.0	26					
^{161}Dy	25.655	(4 4 4)	17.95	−15.7	26	0.7	5.6	3.7	3.2	11
		(18 12 6)	87.25	0.0	16					

[a] Due to different asymmetry factors for the two crystals, the spatial size of the transmitted beam will be increased relative to the spatial acceptance in accordance with eq. (2.10).
[b] Size of projection of X-rays onto crystal surface assumes 1.0 mm spatial acceptance.
[c] For the sake of comparison, the range of integration is unrestricted. Of course, in practice, the integrand is weighted by the incident brightness function to obtain measurable results.

the first crystal uses an asymmetrically cut silicon (4 4 0) reflection with an asymmetry factor of $b_1 = 0.04$ at 14.413 keV. The second crystal uses a reflection with the largest available Bragg angle at this energy in silicon, viz. (9 7 5). The different simulations correspond to different asymmetry factors for the (9 7 5) reflection with values ranging from $b_2 = 1$ to $b_2 = 4$. The conclusion that may be drawn, in this case, is that increasing the asymmetry factor of the (9 7 5) reflection crystal from $b_2 = 1$ to $b_2 = 4$ produces better energy resolution at the cost of a slight decrease in the transmission at the design energy. Table 1 presents transmission-optimized high-resolution monochromators for different nuclear resonances in the energy range 10–30 keV. In the table, $\Delta\Theta$ represents the angular acceptance of the monochromator. Also in the table, ΔE represents the energy acceptance of the monochromator assuming X-ray beams of sufficiently narrow horizontal divergence. The actual transmitted energy bandwidth may be different depending on such source characteristics as vertical and horizontal divergences. Also, only silicon monochromators are presented in the table. It may be possible, if the crystal quality is sufficient, to employ germanium single crystals at higher energies with the advantage of increased efficiency due to larger angular acceptances.

For the purposes of applications, it may be preferable to reduce the energy bandwidth while preserving the remainder of the phase-space configuration of the incident beam. This means preserving the direction of the incident beam and not altering the

size or divergence of the beam beyond the acceptance of the monochromator. This may be performed with two additional crystals that use the same reflections, but opposite asymmetry angles as the first two crystals. By placing them in a $(+\mathrm{l}, +\mathrm{h}, -\mathrm{h}, -\mathrm{l})$ configuration, the initial beam direction is regained along with the size and divergence consistent with the acceptance of the monochromator. This configuration is shown in figures 5(b) and (d).

The four-crystal geometry preserves beam size and direction at the cost of reduced transmission, increased design complexity, and a somewhat smaller ratio of integrated transmission to energy acceptance. The reduced transmission results from additional crystal reflections with less than unit reflectivity. The increased design complexity results from the need to control the position and angle of four crystals instead of just two. This may be partly overcome by designing the four crystals from two monoliths, each monolith having a channel cut through the crystal. Using the resulting two inside parallel faces as the $(+\mathrm{l}, -\mathrm{l})$ and $(+\mathrm{h}, -\mathrm{h})$ components of the monochromator, these two "channel-cut" crystals are nested within each other in a manner consistent with figures 5(b), (d). The end result is a four-crystal high-resolution monochromator that only requires as much angular control as the simpler, two-crystal configuration. Figure 7 shows a plot of the transmission function for a transmission-optimized monochromator designed for 14.413 keV. The high-resolution monochromator uses a symmetric silicon (10 6 4) channnel-cut crystal nested within an asymmetrically cut silicon (4 2 2) channnel-cut crystal.

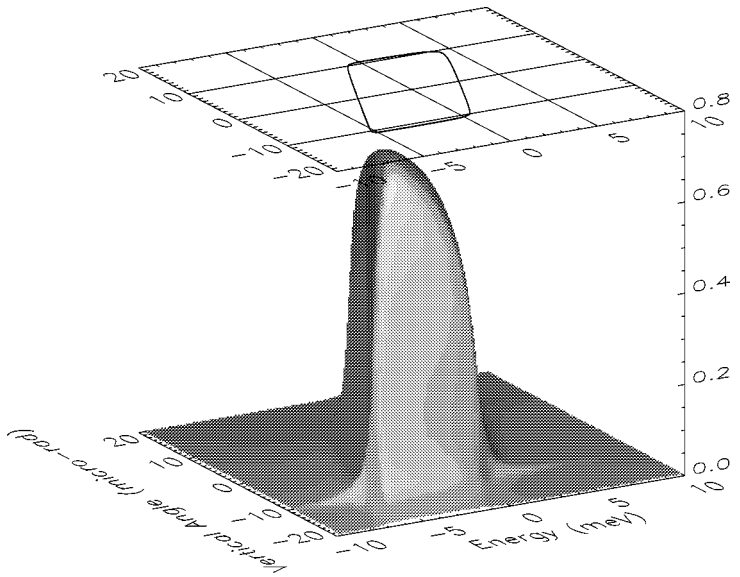

Figure 7. Transmission function $T_\sigma(\theta, \varepsilon)$ around $E_0 = 14.413$ keV for a tansmission-optimized high-resolution monochromator that is composed of silicon (4 2 2)–(10 6 4)–(10 6 4)–(4 2 2) crystal reflections in a $(+, +, -, -)$ scattering geometry. $b_1 = {b_4}^{-1} = 0.0726$ and $b_2 = {b_3}^{-1} = 1.0$. The energy acceptance is 6 meV.

Due to the similarity to the two-crystal geometry discussed above, many of those results also apply in the "nested" case. Thus, the four-crystal versions of the monochromators shown in table 1 will have very similar characteristics, with the exception of a slightly better energy resolution and slightly less integrated transmission. There are a few additional considerations that warrant discussion. Because one channel-cut crystal is "nested" within another channel-cut crystal, size considerations can (and usually do) become a factor. The size of a channel-cut crystal should be kept to a minimum in order to limit the effects of a lack of long-range crystallinity, which may be due to strain, temperature variations, or crystal quality. Restricting the size of the outer channel-cut crystal places constraints on the size of the inner channel-cut crystal and, in turn, on the possible asymmetry factors that can be used for both crystals.

A problem arises from the existence of alternate reflections that may also transmit quasi-monochromatic radiation through an individual channel-cut crystal. This problem can be mitigated by choosing an appropriate zone for the scattering plane. The optimal zone for the scattering plane is the one that possesses the smallest number of alternate reflections lying near the Ewald sphere. Between choosing the primary lattice reflection with its asymmetry angle, and choosing the scattering plane to lie within an optimal zone, the orientation of the crystal with respect to the incident beam direction is completely fixed. This orientation forms the basis for the actual cutting of the crystal.

The transmission-optimized design for high-resolution monochromatization has been successfully demonstrated at nuclear resonant energies in ^{57}Fe [18–20], ^{119}Sn [19, 21,22], and ^{151}Eu [23,24].

4.2. Energy-resolution-optimized design

For experiments that require the best available energy resolution of a monochromator, there is an alternative design to the one discussed above. In the energy range of 5–20 keV, a different approach gives better energy resolution while still maintaining an angle-integrated transmission that is suitable for high-brilliance sources. In the following, this alternative approach is discussed, and a table is assembled containing monochromator designs for nuclear resonances below 20 keV.

One can significantly improve the use of two high-order crystal reflections placed in a $(+,+)$ scattering geometry (cf. figure 4) by asymmetrically cutting the crystals in an appropriate manner. By choosing crystal reflections with the largest possible Bragg angle at the target energy and cutting them as shown in figure 8(a), one can improve the performance of the monochromator by more than an order of magnitude [17]. That is, the ratio of angle-integrated transmission to energy acceptance will improve by more than a factor of ten. This is a significant improvement and, at present, offers the best energy resolution in a two-crystal design that is obtainable in this energy range.

A demonstration of this fact can be carried out by simulating the angle-integrated transmission of two high-order crystal reflections in a $(+\mathrm{h},+\mathrm{h})$ scattering geometry as a function of their asymmetry angles. To improve the angular acceptance and the energy resolution of the $(+\mathrm{h},+\mathrm{h})$ crystal setup, the first crystal must have a negative

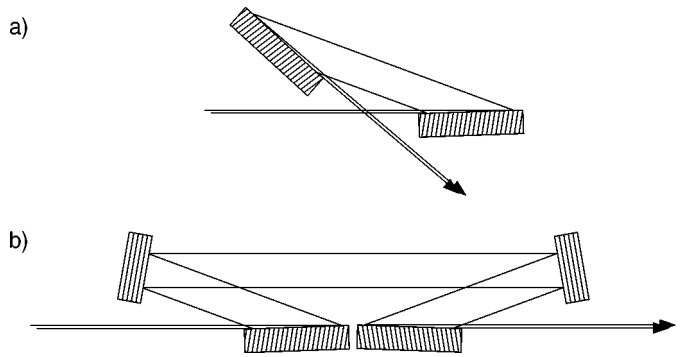

Figure 8. High-resolution monochromators optimized for energy resolution: (a) two asymmetrically cut, high-order, crystal reflections placed in a $(+,+)$ scattering geometry, and (b) a four-reflection version that redirects the beam to the forward direction.

asymmetry angle. Recall that a negative asymmetry angle means the incident X-rays must make an angle with respect to the crystal surface that is less than the Bragg angle. To further improve the energy resolution, the second crystal must also be cut asymmetrically, but with a positive asymmetry angle. The optimal value to choose for the asymmetry angle of the second crystal depends on a number of factors, but its magnitude should not be greater than the magnitude of the asymmetry angle for the first crystal. This allows proper divergence matching between the first and second crystals. For our purposes, however, it is sufficient to simply assume that the two crystal reflections have equal and opposite asymmetry angles. For the simulation, crystal reflections in silicon with the largest available Bragg angle at 14.413 keV are used, viz., (9 7 5). Calculating the transmission function for σ-polarized X-rays and subsequently integrating over the angle variables yields figure 9. The lowest peak angle-integrated transmission is for the symmetrically cut case. By gradually increasing the asymmetry angles on both crystals, the angle-integrated transmission on the energy scale becomes sharper with increased peak angle-integrated transmission at the target energy. For the symmetric case, the energy acceptance is 3.4 meV and the peak angle-integrated transmission is 1.1 μrad, while at the extreme asymmetric case ($b_1 = {b_2}^{-1} = 0.05$), the energy acceptance is 0.8 meV and the peak angle-integrated transmission is 2.7 μrad. The ratio of angle-integrated transmission to energy acceptance increased by more than a factor of ten by asymmetrically cutting the crystals. This is a general feature of cutting the crystals asymmetrically as in figure 8(a). At other energies, by using different crystal materials and/or different crystal reflections, the improvement may be more or less than the above case, but the result will always be a better monochromator. It is also noteworthy that the tails of the angle-integrated transmission function decreased significantly for the asymmetric case, thus allowing inelastic nuclear resonant scattering measurements to obtain reliable information at very low energy transfers.

The actual choice of crystal reflections and asymmetry angles depends on the intended purpose and the available angular control. In general, if energy resolution is

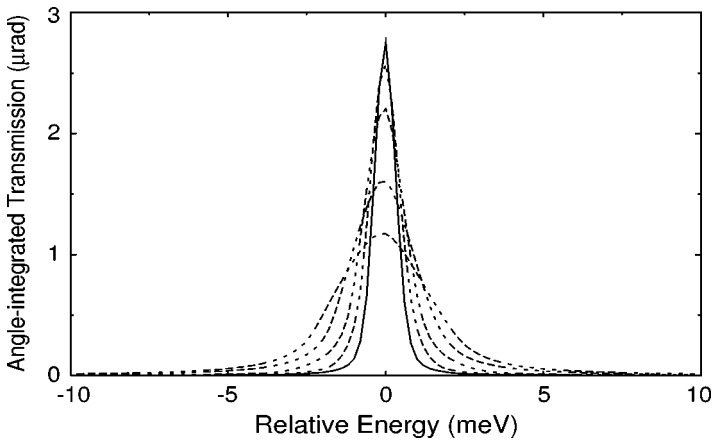

Figure 9. Angle-integrated transmission $\int T_\sigma(\theta,\varepsilon)\,\mathrm{d}\theta$ as a function of energy (relative to 14.413 keV) for two silicon (9 7 5) reflections in a $(+,+)$ geometry as shown in figure 8(a). The crystals with larger (opposite) asymmetry cuts produce better energy resolution with enhanced transmission at the design energy: $b_1 = 1/b_2 = 1, 0.5, 0.2, 0.1, 0.05$.

of paramount concern, both crystal reflections should have the largest available Bragg angle for a given energy. As for the asymmetry angles, the incident angle on the first crystal should remain well away from the critical angle for total external reflection. Extreme asymmetry angles that approach the critical angle for total external reflection result in a saturation of the Darwin width, as well as a reduction of the efficiency due to flux lost to the specular beam [25]. The incident angle on the first crystal should be less than 1.0° for energies in this range, but should be greater than twice the critical angle for total external reflection (i.e., $2\theta_\mathrm{c} < \Theta + \alpha_1 < 1.0^\circ$). For the asymmetry angle on the second crystal, various choices should be simulated to determine the value that gives the best ratio of integrated transmission to energy acceptance. The best choice for the asymmetry angle of the second crystal turns out to be a value with magnitude somewhat less than that chosen for the first crystal.

Such a high-resolution monochromator has been constructed for the 14.413 keV nuclear resonance in ^{57}Fe. The key parameters that were settled upon are offered as an example. The crystal reflection in silicon with the largest Bragg angle (80.4°) at this energy is the (9 7 5). The asymmetry angle for the first crystal was chosen to be -79.6°, which results in an asymmetry factor of 0.04. This makes the minimum size of the first crystal needed for a spatial acceptance of 1.0 mm only 72 mm long. The asymmetry angle for the second crystal was chosen to be $+78.5^\circ$. The minimum size is then 69 mm long for the second crystal. The transmission function for two silicon (9 7 5) crystal reflections in a $(+,+)$ scattering geometry and with the above asymmetry angles is shown in figure 10. The energy acceptance of the monochromator is 0.94 meV and the peak angle-integrated transmission is 3.8 μrad (angular acceptance = 9.1 μrad).

The results of designing monochromators at other nuclear resonances below 20 keV are shown in table 2. For the cases in table 2, the incident angle on the

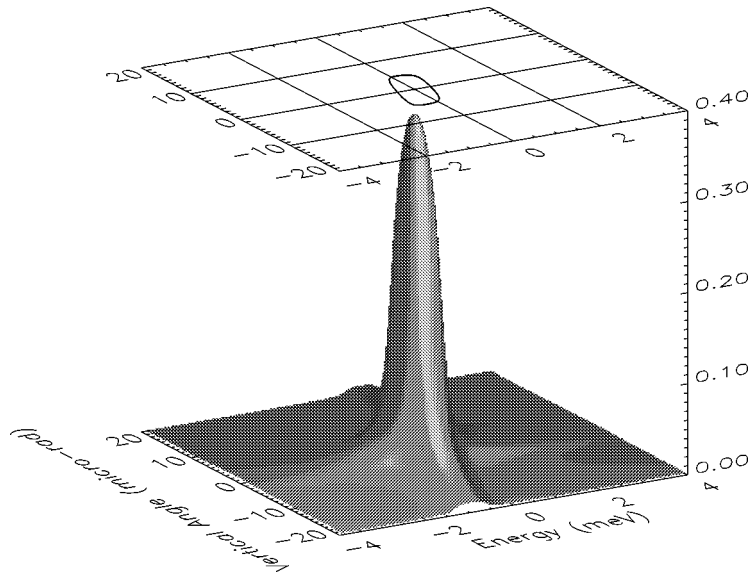

Figure 10. Transmission function $T_\sigma(\theta, \varepsilon)$ around $E_0 = 14.413$ keV for a resolution-optimized high-resolution monochromator that is composed of two silicon (9 7 5) crystal reflections in a $(+,+)$ scattering geometry. The crystals have asymmetry factors of $b_1 = 0.040$ and $b_2 = 10.4$. The energy acceptance is 0.91 meV.

first crystal is chosen to be $\approx 0.8^\circ$ (i.e., $\alpha_1 \approx 0.8^\circ - \Theta$). This gives good angular acceptance without severe absorption and also keeps the crystal size at a reasonable length. Note that for the lower energies, where angular acceptances of silicon crystal reflections are large compared to the divergences of present-day synchrotron sources, equal and opposite asymmetry angles were given to the two crystals. This is because the exact divergence matching condition between the crystals does not require exacting angular resolution. The actual choice of asymmetry angles may not be optimal in all cases, since the best choice invariably depends on the characteristics of the radiation source. Instead, the table represents typical design parameters along with the resulting performances that can be expected at the different energies.

Above 20 keV, angular tolerances (10^{-8} rad) and required temperature stability (10^{-3} K) become extreme, while angular acceptances remain at a somewhat uninviting few μradian. In addition, crystal perfection ($d/\Delta d$) may very well become an overriding constraint since the energy resolutions ($E/\Delta E$) involved approach 10^8–10^9. If crystal quality does not preclude the use of this design above 20 keV, then it may be possible to both alleviate thermal problems and, at the same time, improve the efficiency of high-resolution monochromators by cooling them. In the case of silicon, the coefficient of thermal expansion goes to zero at a temperature of approximately 123 K [26]. Thus, cooling the optic to that temperature results in a significantly reduced sensitivity to thermal gradients. Furthermore, cryogenically cooling the silicon crystals would result in a dramatic increase in the Debye–Waller factor, especially for high-order reflections. This results in enhanced efficiency because the reflectivities (cf.

Table 2
Silicon two-crystal high-resolution monochromators of the energy-resolution-optimized design for different nuclear resonances below 20 keV. The chosen asymmetry angles (α) should be considered representative rather than optimal.

Isotope	E_0 (keV)	$\vec{H}$ (h k l)	Θ_B (deg.)	α (deg.)	s (mm)	ΔE (meV)	$\Delta\Theta$ (μrad)	$\int T_\sigma \, \mathrm{d}\theta^a$ (μrad)	$\int T_\sigma \, \mathrm{d}\theta \, \mathrm{d}\varepsilon^a$ (nrad-eV)	δT_0 (mK)
^{181}Ta	6.214	(3 3 3)	72.6	−71.8	70	7.1	170	32.0	310	465
		(3 3 3)		+71.8	70					
^{169}Tm	8.410	(5 5 1)	75.8	−75.0	76	3.4	73	18.7	85.1	158
		(5 5 1)		+75.0	76					
^{83}Kr	9.410	(7 3 3)	83.2	−82.4	75	3.1	66	23.7	96.4	133
		(7 3 3)		+82.4	75					
^{133}Ba	12.290	(9 5 3)	84.9	−84.1	72	1.6	25	9.7	17.5	51
		(9 5 3)		+84.0[b]	71					
^{73}Ge	13.263	(9 5 5)	80.1	−79.3	74	1.2	13	5.3	7.7	35
		(9 5 5)		+78.3[b]	71					
^{57}Fe	14.413	(9 7 5)	80.4	−79.6	72	0.91	9.1	3.8	4.5	25
		(9 7 5)		+78.5[b]	69					

[a] For the sake of comparison, the range of integration is unrestricted. Of course, in practice, the integrand is weighted by the incident brightness function to obtain measurable results.
[b] Due to the different asymmetry angles, the spatial size of the transmitted beam will be increased relative to the spatial acceptance in accordance with eq. (2.10).

eqs. (2.1)–(2.2)) as well as the angular acceptances (cf. eq. (2.4)) are proportional to the Debye–Waller factor. It turns out that the energy resolution is slightly degraded by cooling the crystals, because the energy resolution is approximately proportional to the Darwin width in the resolution-optimized design. The trade-off between efficiency and resolution is heavily favored for efficiency though, because the ratio of integrated transmission to energy acceptance can improve by a factor of ten in some cases by cooling the monochromator. The major drawback, at present, of cryogenically cooling the silicon crystals is the difficulty in doing so while maintaining sub-μradian angular stability.

An extension of the two-crystal (+h, +h) design discussed above is a four-crystal design of a (+h, −h, +h, −h) scattering geometry depicted in figure 8(b). This preserves the beam direction, as well as other aspects of the transverse phase space. Due to the extreme asymmetry angles, the reflectivities are typically much less than one. Therefore, using a combination of asymmetrically cut crystals with symmetrically cut crystals generally produces significantly enhanced efficiency.

The resolution-optimized design discussed in this section has been successfully demonstrated at the 14.413 keV nuclear resonance in ^{57}Fe using two reflections to obtain 1.65 meV [27], and two extremely asymmetric reflections to obtain 0.92 meV [28] and 0.65 meV [29]. At 14.413 keV, the limit to energy bandwidth from this design

using silicon is approximately 0.3 meV. Over the extended energy range of 5–30 keV, the degree of energy resolution depends in part on the extinction depth for the crystal reflections. Consequently, for lower energies in this range where extinction depths are small, energy resolutions become somewhat worse but are still in the meV energy range. Conversely, for higher energies in this range where extinction depths are large, this design offers the potential for even better energy resolutions.

A variation on the designs mentioned above will result in a polarizing monochromator. If at least one of the reflections of the design is chosen with a Bragg angle close to 45°, it is possible to produce a high-resolution monochromator that also acts as a linear polarization filter [30]. This has significant advantages for experiments that need X-rays with both high energy resolution and high polarization purity. Polarizing high-resolution monochromators have been successfully made for ^{57}Fe [30], and ^{151}Eu [23].

4.3. Practical considerations and characterization

Even with the crystal reflections and the approximate asymmetry factors determined, additional design considerations need to be taken into account such as the size of the crystals, the required angular control, and the need for temperature stability.

The size of crystals needed is affected strongly by the source characteristics, as well as by the individual asymmetry factors. First, the maximum acceptable beam size is typically not determined by the size of the crystal but by its angular acceptance (D_-), its distance from the source (L), and the source size (Σ_0). If, in addition, one includes a non-zero energy width ΔE of the radiation, then the maximum acceptable beam size is determined by the following expression:

$$S_- = L\left(D_- + \frac{\Delta E}{E\cot\Theta}\right) + \Sigma_0. \tag{4.4}$$

Notice that the distance from the source should be kept small when possible as this results in smaller sizes for diffracting crystals. Second, the size of the first crystal (s_1) needed to properly diffract a beam of this size may be determined from the following expression:

$$s_1 = \frac{(S_-)_1}{\sin(\Theta_1 + \alpha_1)}. \tag{4.5}$$

The size of the beam after the first crystal may be determined from eq. (2.10). The size of the second crystal (s_2) needed to properly diffract this beam can similarly be determined from

$$s_2 = \frac{(S_-)_2}{\sin(\Theta_2 + \alpha_2)}. \tag{4.6}$$

This may be extended in a similar way for any additional crystal faces that are close to each other; otherwise beam divergence needs to be considered.

As one attempts to achieve ever smaller energy bandwidths, the question of the stability of a given energy alignment to relative changes in crystal temperature needs to be addressed. If the temperature of a crystal changes by an amount δT, the effect is manifested in the spacing of the diffraction planes. Depending on the sign of the coefficient for thermal expansion β, a positive δT may result in an increase or decrease of the diffraction plane spacing. If a high-resolution monochromator possesses an energy bandwidth of ΔE, then the amount the temperature must change in order for the energy alignment to change by that same amount is given by

$$\delta T_0 = \frac{1}{\beta}\frac{\Delta E}{E}. \tag{4.7}$$

For silicon at room temperature, $\beta = 2.56\times10^{-6}\ K^{-1}$ [31]. This implies, for example, that a silicon high-resolution monochromator with a $\Delta E = 1$ meV at 14.413 keV will incur an energy shift of a very perceptible 1 meV if all of its crystals change by 0.027 K. If δT_0 is so small as to require energy re-alignments to accommodate temperature drifts, then the angle adjustments needed for each crystal are simply given by the following for a two-crystal system in a $(+,+)$ geometry:

$$\begin{pmatrix}\delta\theta_1\\ \delta\theta_2\end{pmatrix} = -\beta\begin{pmatrix}\tan\Theta_1 & 0\\ 2\tan\Theta_1 & \tan\Theta_2\end{pmatrix}\begin{pmatrix}\delta T_1\\ \delta T_2\end{pmatrix}, \tag{4.8}$$

where $\delta\theta_i$ is defined as the change in the angle of the ith crystal necessary to maintain energy alignment. Note that a positive value of $\delta\theta_i$ results in an increase in the scattering angle at the ith crystal. One may generalize this for N crystals of different materials in series and obtain

$$\delta\theta_n = -\sum_{i=1}^{n} C_{ni}2^{n-i}\beta_i\tan\Theta_i\delta T_i \quad (1\leqslant n\leqslant N), \tag{4.9}$$

where C_{ni} is defined as

$$C_{ni} = \begin{cases} 1 & \text{if } i = n,\\ 0 & \text{if } i > n,\\ \pm1 & \text{if } i < n \text{ and } i\text{th crystal is } (+,\pm) \text{ rel. to } (i-1)\text{th crystal.}\end{cases} \tag{4.10}$$

The sources of uncertainty in the Bragg angle $\delta\theta_0$ include strain in the crystal and nonuniformity of the asymmetry angle over the diffracting surface. The scattering angle of the beam from a crystal depends on the asymmetry factor. This is clear from figure 2 and calculable from eqs. (2.8) and (2.9). As a result, the scattering angle is sensitive to variations in the asymmetry factor. Thus, a spread in the asymmetry factor will result in a spread of the diffracted beam divergence from a crystal. If this spread in the diffracted beam divergence is great enough, the effect is either a loss of transmission and/or an increased energy acceptance. To calculate the sensitivity of the diffracted beam divergence to variations in the asymmetry angle, α, one can

differentiate the angular shift due to refraction, $\Delta_\pm$, with respect to the asymmetry angle and obtain

$$\frac{\partial\Delta_\pm}{\partial\alpha} = \frac{\partial\Delta_\pm}{\partial b}\,\frac{\partial b}{\partial\alpha} = \pm\frac{\Delta_S}{2}\left(\frac{b^{\pm1}}{b}\right)\left(\frac{\sin(2\Theta)}{\sin^2(\Theta-\alpha)}\right). \tag{4.11}$$

Using these relations, the spread in the angle of the diffracted (acceptance) beam due to variations in the asymmetry angle, $\delta\alpha$, is

$$\delta\Delta_\pm = \frac{\partial\Delta_\pm}{\partial\alpha}\,\delta\alpha. \tag{4.12}$$

By requiring the angular spread of the diffracted (acceptance) beam to be small compared to the angular width due to extinction, one obtains a constraint on the surface flatness of the diffracting crystal of

$$\delta\alpha_o \ll \left(\frac{\partial\Delta_\pm}{\partial\alpha}\right)^{-1} D_\pm. \tag{4.13}$$

Due to angular tolerances that can be quite small, e.g., 0.1 μrad, typical values for $\delta\alpha_0$ are on the order of 10^{-3} rad for the transmission-optimized design and as low as 10^{-4} rad for the energy-resolution-optimized design.

Characterizing the performance of a monochromator begins with a measurement of two quantities: the energy-resolution function and the ratio of fluxes before and after the monochromator. There are, of course, other performance criteria, such as tunability and long-term stability, but these are of secondary importance. The energy-resolution function $\mathcal{R}(\varepsilon)$ gives the distribution of spectral flux and is calculated by performing an integration over angle of the spectral-brightness function and summing over the polarizations,

$$\mathcal{R}_1(\varepsilon) = \sum_\lambda \int B_1^{(\lambda)}\big(\theta',\varepsilon\big)\,\mathrm{d}\theta' = \sum_\lambda \int T^{(\lambda)}(\theta,\varepsilon)B_0^{(\lambda)}(\theta,\varepsilon)\,\mathrm{d}\theta, \tag{4.14}$$

where $B_0^{(\lambda)}$ refers to the λ-polarization component of the spectral-brightness function before the monochromator and $B_1^{(\lambda)}$ is the λ-polarization component of the spectral-brightness function after. The energy bandwidth is then just the width of the energy-resolution function. Experimentally, it is possible to make a direct measurement of the energy-resolution function with the use of coherent elastic nuclear resonant scattering (see, e.g., [19]). Thus, in the case of nuclear resonant scattering, one can make a direct comparison between the measured energy-resolution function and that which is calculated from eq. (4.14). For the ratio of fluxes before and after the monochromator, the theoretically expected value is given by

$$\frac{\mathcal{F}_1}{\mathcal{F}_0} = \frac{\sum_\lambda \int B_1^{(\lambda)}(\theta',\varepsilon)\,\mathrm{d}\theta'\,\mathrm{d}\varepsilon}{\sum_\lambda \int B_0^{(\lambda)}(\theta,\varepsilon)\,\mathrm{d}\theta\,\mathrm{d}\varepsilon} = \frac{\sum_\lambda \int T^{(\lambda)}(\theta,\varepsilon)B_0^{(\lambda)}(\theta,\varepsilon)\,\mathrm{d}\theta\,\mathrm{d}\varepsilon}{\sum_\lambda \int B_0^{(\lambda)}(\theta,\varepsilon)\,\mathrm{d}\theta\,\mathrm{d}\varepsilon}. \tag{4.15}$$

So, by comparing the theoretical value to the experimental value for these two quantities (the energy-resolution function and the ratio of fluxes before and after the monochromator), one can determine the quality of the X-ray optic.

Measurements of the energy-resolution function of the multicrystal arrangement requires careful angular alignment to guarantee accurate results. The Bragg angle refers to a rotation angle about an axis that is perpendicular to the scattering plane. This requires the best angular resolution of all rotational alignments and needs to be better than the divergence of the monochromatic radiation between the two crystals. The other two rotation axes both lie in the scattering plane. For the purpose of discussion, these two axes are taken to be that which is parallel to the lattice vector associated with the crystal reflection and that which is perpendicular to the lattice vector and parallel to the scattering plane. For the rotation about the lattice vector, the angular resolution is of no concern for symmetrically cut crystal reflections since the transmission characteristics of the X-rays are independent of the rotation as long as other lattice reflections remain off the Ewald sphere. For asymmetrically cut crystal reflections, the transmission characteristics of the X-rays are affected by a rotation about the lattice vector because the actual asymmetry parameter varies with the rotation. The sensitivity of this rotational alignment (ϕ) is somewhat coarse and is proportional to the asymmetry angle (α) itself by $\delta\alpha/\delta\phi = 2\alpha/\pi$. In practice, variations of the rotation angle about the lattice vector should be less than 10 mrad for crystal reflections with large asymmetry angles. The third and last rotational alignment that needs to be considered is the one about an axis that is perpendicular to the lattice vector and parallel to the scattering plane. This will be referred to as the tilt adjustment. The sensitivity of this angular alignment depends on a number of variables, including the vertical and horizontal angular acceptances of the crystal reflection, and the vertical and horizontal angular divergences of the X-rays that are incident. The angular resolution required for the tilt adjustment is typically 10^{-3}–10^{-4} rad.

Energy scanning of a two-crystal monochromator is accomplished by rotating the crystals, as well as monitoring their temperatures. For two crystals of the same material placed in a $(+,+)$ scattering geometry, the conversion from relative rotation angle and temperature of the two crystals to relative energy is given by

$$\delta E = \frac{E_0 \cdot (\delta\theta_1 - \delta\theta_2 - \beta \cdot (\delta T_1 \tan\Theta_1 + \delta T_2 \tan\Theta_2))}{\tan\Theta_1 + \tan\Theta_2}, \tag{4.16}$$

where β is the coefficient of thermal expansion, and the energy (δE), angles ($\delta\theta_i$), and temperatures (δT_i) are referenced from their values at some known energy reference (E_0). In the case of nuclear resonant scattering, this energy reference is the nuclear resonance itself.

Different methods of monochromatizing synchrotron radiation for the purposes of performing nuclear resonant scattering experiments have been presented. For experiments that need as much spectral flux as possible with reasonably high energy resolution, a transmission-optimized design achieves a few meV energy resolution in the 10–20 keV energy range and reaches to sub-meV energy resolution in the 20–30 keV

energy range. For experiments requiring the highest energy resolution at a given energy with modest transmission, the energy-resolution-optimized design achieves a few meV energy resolution even in the 5–10 keV energy range and reaches to sub-meV in the 10–20 keV energy range. The most suitable design depends on the energy and the application. Both of these designs rely on the use of high-quality crystalline silicon but can be implemented with other crystalline materials of sufficient quality. The level of resolution that has been obtained so far using silicon does not appear to be limited by the available crystal quality. In their respective energy ranges, these designs provide reasonable efficiency with high resolution at present-day third-generation synchrotron sources. In the future, it may be possible to extend the applicable energy ranges of these designs to higher energies and higher energy resolutions with sufficient motion control, temperature control, and crystal preparation. At higher energies, such designs would have a relatively low efficiency for present-day sources, but more brilliant sources would make them more efficient and might offer the possibility of performing X-ray spectroscopy with significantly improved resolution.

Acknowledgements

The author would like to thank E.E. Alp, G. Bortel, M.Y. Hu, and W. Sturhahn at the Advanced Photon Source for fruitful discussions. The U.S.-DOE provided financial support for this work under contract BES Materials Science W-31-109-ENG-38.

References

[1] C.G. Darwin, Phil. Mag. 27 (1914) 315; Phil. Mag. 27 (1914) 675.
[2] P.P. Ewald, Ann. Physik 49 (1916) 1; Ann. Physik 49 (1916) 117; Ann. Physik 54 (1917) 519.
[3] M. von Laue, Ergeb Exakt. Naturw. 10 (1931) 133.
[4] W.H. Zachariasen, *Theory of X-ray Diffraction in Crystals* (Wiley, New York, 1945).
[5] B.W. Batterman and H. Cole, Rev. Mod. Phys. 36 (1964) 681.
[6] B.E. Warren, *X-ray Diffraction* (Addison-Wesley, Reading, MA, 1969); (Dover, New York, 1990).
[7] S. Kikuta, J. Phys. Soc. Jpn. 30 (1971) 222.
[8] T. Matsushita and H. Hashizume, *Handbook of Synchrotron Radiation*, Vol. 1, ed. E.E. Koch (1983) p. 261.
[9] J.A. Ibers and W.C. Hamilton, eds., *International Tables for X-ray Crystallography*, Vols. 2, 4 (The Kynoch Press, Birmingham, 1974).
[10] D.T. Cromer and D. Liberman, J. Chem. Phys. 53 (1970) 1891.
[11] T.J. Davis, J. X-ray Sci. Technol. 2 (1990) 180.
[12] A. Caticha and S. Caticha-Ellis, Phys. Rev. B 25 (1982) 971.
[13] Yu.V. Shvyd'ko, E. Gerdau, J. Jäschke, O. Leupold, M. Lucht and H.D. Rüter, Phys. Rev. B 57 (1998) 4968.
[14] E. Burkel, *Inelastic Scattering of X-rays with Very High Energy Resolution* (Springer, New York, 1991).
[15] G. Faigel, D.P. Siddons, J.B. Hastings, P.E. Haustein, J.R. Grover, J.P. Remeika and A.S. Cooper, Phys. Rev. Lett. 58 (1987) 2699.
[16] T. Ishikawa, Y. Yoda, K. Izumi, C.K. Suzuki, X.W. Zhang, M. Ando and S. Kikuta, Rev. Sci. Instrum. 63 (1992) 1015.

[17] T.S. Toellner, Ph.D. dissertation, Northwestern University (June 1996).
[18] T.S. Toellner, T. Mooney, S. Shastri and E. Alp, in: *Optics for High-Brightness Synchrotron Radiation Beamlines*, ed. J. Arthur, Proceedings of SPIE 1740 (1993) 218.
[19] T.M. Mooney, T.S. Toellner, W. Sturhahn, E.E. Alp and S.D. Shastri, Nucl. Instrum. Methods A 347 (1994) 348.
[20] A.I. Chumakov, R. Rüffer, A.Q.R. Baron, H. Grünsteudel and H.F. Grünsteudel, Phys. Rev. B 54 (1996) 9596.
[21] A.I. Chumakov, A. Barla, R. Rüffer, J. Metge, H.F. Grünsteudel, H. Grünsteudel, J. Plessel, H. Winkelmann and M.M. Abd-Elmeguid, Phys. Rev. B 58 (1998) 254.
[22] M.Y. Hu, T.S. Toellner, W. Sturhahn, P.M. Hession, J.P. Sutter and E.E. Alp, Nucl. Instrum. Methods A 430 (1999) 271.
[23] O. Leupold, J. Pollman, E. Gerdau, H.D. Rüter, G. Faigel, M. Tegze, G. Bortel, R. Rüffer, A.I. Chumakov and A.Q.R. Baron, Europhys. Lett. 35 (1996) 671.
[24] P. Hession et al., Argonne National Laboratory (1998, unpublished).
[25] S. Kimura, J. Harada and T. Ishikawa, Acta. Cryst. A 50 (1994) 337.
[26] *Properties of Silicon*, EMIS Datareviews Series No. 4 (INSPEC, The Institution of Electrical Engineers, London and New York, 1988).
[27] A.I. Chumakov, J. Metge, A.Q.R. Baron, H. Grünsteudel, H.F. Grünsteudel, R. Rüffer and T. Ishikawa, Nucl. Instrum. Methods A 383 (1996) 642.
[28] T.S. Toellner, M.Y. Hu, W. Sturhahn, K. Quast and E.E. Alp, Appl. Phys. Lett. 71 (1997) 2112.
[29] T.S. Toellner et al., Argonne National Laboratory (1997, unpublished).
[30] D.P. Siddons, U. Bergmann and J.B. Hastings, Phys. Rev. Lett. 70 (1993) 359.
[31] R.D. Deslattes, Ann. Phys. 129 (1980) 378.